Stardust Wild 2 Dust Measurements

Book Section

STARDUST WILD 2 DUST MEASUREMENTS

S.F. Green[(1)], N. McBride[(1)], M.T.S.H. Colwell[(1)], J.A.M. McDonnell[(1)], A.J. Tuzzolino[(2)], T.E. Economou[(2)], B.C. Clark[(3)], Z. Sekanina[(4)], P. Tsou[(4)], D.E. Brownlee[(5)]

[(1)]Planetary and Space Sciences Research Institute, The Open University, Walton Hall, Milton Keynes, MK76AA, UK, Email: s.f.green@open.ac.uk.
[(2)]Laboratory for Astrophysics and Space Research, Enrico Fermi Institute, University of Chicago, 933 East 56th St, Chicago Ill 60637, USA.
[(3)] Lockheed Martin Astronautics, P.O. Box 179, MS-B0560, Denver, CO 80201, USA.
[(4)] Jet Propulsion Laboratory, California Institute of Technology, 4800 Oak Grove Drive, Pasadena CA 91109, USA.
[(5)] Astronomy Department, University of Washington, bx 351580, Seattle, WA 98195, USA.

ABSTRACT

During its passage through the coma of comet 81P/Wild 2 in January 2004 to collect dust particles for return to the Earth, instruments on Stardust made extensive measurements of the dust coma environment. The inner coma was characterized by many narrow jets, imaged by the Navigation Camera. Dust fluxes measured by the Dust Flux Monitor Instrument (DFMI) revealed a highly non-uniform spatial distribution, with short duration bursts of impacts implying localized spatial density changes of orders of magnitude on scales of less than a km as well as a second period of high activity ~4000 km from the nucleus where almost 80% of the detected impacts occurred. The Cometary and Interstellar Dust Analyzer (CIDA) obtained 29 dust impact mass spectra near closest approach. The spacecraft Attitude Control System (ACS) detected one event attributable to a large particle impact.

The overall mass distribution in the inner coma was dominated by the largest grains, with an average cumulative mass distribution index of α=0.75±0.05 (where the number of particles of mass m or larger, $N(m) \propto m^{-\alpha}$). The mass distribution was consistent with the ACS detection but not with the CIDA results which implied an impact rate a factor of 10^3 lower. The mass distribution was also highly variable during the flyby, and during the second period of high activity, small grains dominated, with α=1.13±0.2.

The enormous variations in dust spatial density over distances of a few hundred metres, have been interpreted as the result of jets and distributed particle fragmentation, with the second period of high activity resulting from outgassing and/or fragmentation of a large (10s of metres diameter) boulder. This interpretation has been received with some skepticism. We review the data, the evidence for fragmentation and refute the criticisms leveled at this interpretation. Data from other comets indicate that the same processes may have occurred and therefore may be common in comets in general.

1. INTRODUCTION

1.1. The dust environment of comet 81P/Wild 2

The primary objective of Stardust is to capture cometary and interstellar dust grains intact and return them to the Earth for in-depth microanalysis [1,2]. Cometary dust particles, trapped in the volatile ices of the nucleus since their formation, contain information on the conditions in the pre-solar nebula, its precursor interstellar cloud and nucleosynthetic processes in the stars from which their constituent grains originally formed. They can be compared with interstellar grains directly sampled from the flow of particles through the Solar System, first detected by the Ulysses spacecraft [3].

Comets are the source of a major component of interplanetary dust. The larger (sub-mm and larger) dust grains leave the nucleus with relatively low velocities, forming cometary dust trails and relatively long lasting meteoroid streams, which gradually dissipate into the zodiacal dust complex, whereas micron sized (and somewhat smaller) grains are rapidly swept out of the inner Solar System by solar radiation pressure. The contribution of comets to the total interplanetary dust complex, and the subsequent dynamics of the individual grains, is critically dependent on the dust mass (or size) distribution. Stardust carried two dedicated experiments for in situ detection of impacting dust particles, as well as a camera for coma imaging. In this paper we summarize the main results from the in-situ dust coma studies and their implications for particle properties and dynamics. The interpretation of these data by widespread fragmentation has been received with some skepticism. The evidence will be reviewed and common criticisms refuted. Comparisons with results from ground- and space-based observations will be assessed to determine if such processes may be common in comets.

1.2. Navigation Camera

The navigation camera (NavCam) [4] was designed to perform the dual function of navigating the spacecraft to its close encounter with P/Wild 2 and take science images of the nucleus near closest approach. The conflicting requirements of navigation and science led to an imaging sequence at encounter with alternating long (0.1s) and short (0.01s) exposures respectively. The long exposures were used to ensure well exposed images for autonomous tracking of the nucleus. Several filters were incorporated in the camera but the filter wheel jammed in flight with a wide band navigation filter in place, giving a wavelength coverage of 500 to 800 nm. Although this prevented separation of the emission from gaseous species, scattering from dust particles was expected to dominate the coma images and provide a global context for the direct sampling of dust particles.

1.3. Dust Flux Monitor Instrument

The objectives of the Stardust Dust Flux Monitor Instrument (DFMI) were to:

- Measure the interplanetary dust flux,
- Determine particle fluxes during the 81P/Wild 2 flyby,
- Determine the particle mass distribution in the coma of 81P/Wild 2,
- To provide the context for the collected dust samples,
- To monitor the dust environment at P/Wild 2 for spacecraft health and interpretation of anomalies.

The DFMI combined two different dust detection techniques incorporated in three independent sensors. PVDF (polyvinylidene fluoride) dust sensors consist of a thin film of permanently polarized material. An impacting dust particle produces rapid local destruction of dipoles, resulting in a short current pulse with maximum amplitude depending on the volume of material destroyed (which depends on the impacting particle mass and speed). Two PVDF sensors with different foil thicknesses and therefore sensitivities, were located on the main shield of Stardust. The dual acoustic sensor system, utilized two piezoelectric crystals mounted on the first two layers of the spacecraft Whipple dust shield to measure the flux of larger particles. Figure 1 illustrates the location of the sensors and the parts of the spacecraft exposed to dust impacts during the encounter. Full details of the instrument design are given in [5].

The limiting particle masses and diameters (calculated assuming spherical particles with density of 500 kg m^{-3}) detectable with each sensor at the Stardust encounter speed are shown in Table 1.

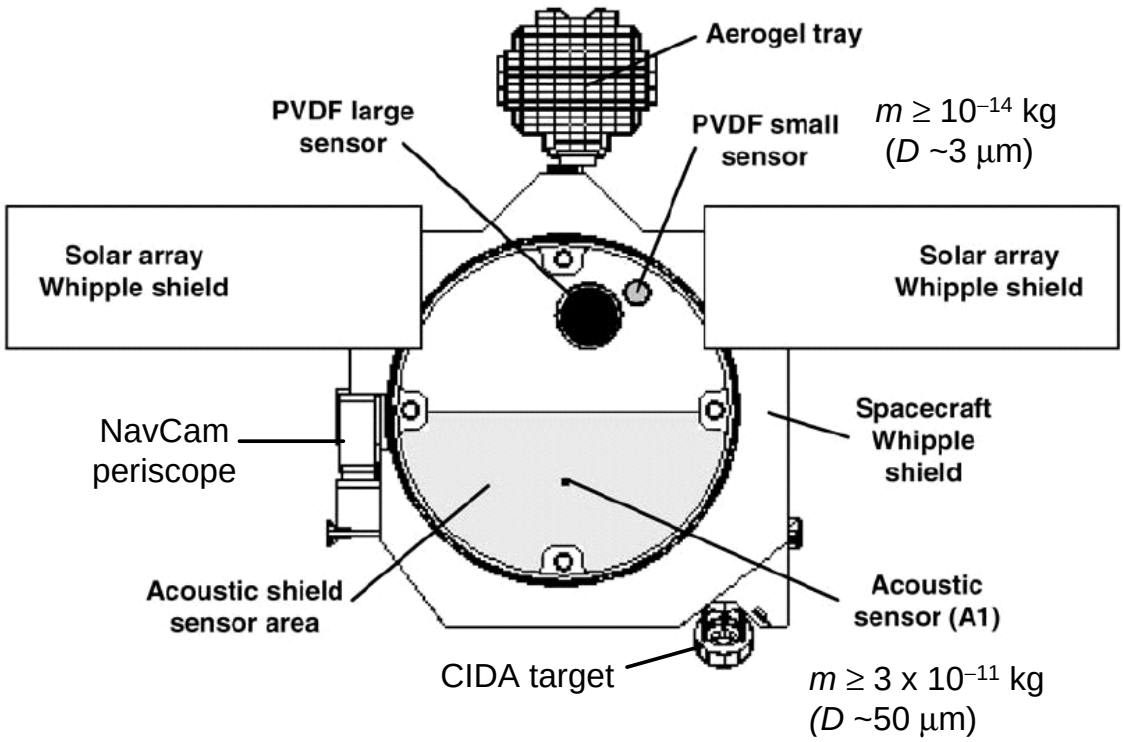

Figure 1. View of the Stardust spacecraft opposite to the direction of its velocity vector at the time of Wild 2 encounter. The rear shield acoustic sensor (A2) is mounted immediately behind the A1 sensor.

Table 1 DFMI sensors

Sensor	No. of channels	Area (m^2)	Limiting mass (kg)	equivalent diameter
PVDF Small	4	0.002	10^{-14}	~ 3 μm
PVDF Large	4	0.02	8.5×10^{-11}	~ 70 μm
Acoustic front (A1)	2	0.1 - 0.3 †	3×10^{-11}	~ 50 μm
Acoustic rear (A2)	2	~0.3	2×10^{-7}	~ 1 mm

† depends on mass distribution.

1.4. Cometary and Interstellar Dust Analyser

The Cometary and Interstellar Dust Analyzer (CIDA) is a time-of-flight mass spectrometer which measured ions produced by dust particles impacting the instrument's target [6]. Its primary objective was the analysis of cometary and interstellar particle compositions, with emphasis on the organic component. First results are presented in [7]. CIDA also had the capability to act as a flux monitor since it incorporated an impact event counter with known dead time. The mass threshold for CIDA was 10^{-15} kg [7] with a maximum effective sensor area of 8.7×10^{-3} m^2 [6].

1.5. Dynamic science

In addition to data from the science instruments, it is possible to determine some information on large impacting particles from perturbations in the spacecraft motion. Although the flyby geometry precluded measurement in the Doppler data of decelerations caused by impacts, the Attitude Control System (ACS) data was sampled at a high rate, permitting detection of large particles if they did not impact in line with the centre of mass. The solar array shields (see Figure 1) provided a cross section of nearly 0.5 m^2 with a moment arm ~1 m or more from the central axis. Random impacts from single large particles of mass greater than ~10^{-6} kg would be detectable by the torque they applied to the spacecraft. A large off-axis impact would have caused the automatic firing of thrusters (either 0.89 N or 4.45 N) to correct the resultant rotation [8].

2. P/WILD 2 ENCOUNTER RESULTS

Stardust successfully completed its flyby of comet 81P/Wild 2 on 2 January 2004 with a closest approach to the nucleus of 236.4 ± 1 km at a relative speed of 6.12 km s^{-1} [9]. Dust impacts were detected by all onboard experiments.

2.1. NavCam coma images

The NavCam acquired 72 images during the close flyby period (closest approach time ± 6 minutes) with solar phase angles ranging from 70º inbound, down to 3º near closest approach and up to 110º outbound.

The short exposure "science" images revealed a unique surface devoid of regolith and with sufficient strength to support steep-walled depressions, layered terrain and pinnacles over 100m in height [10]. Although no nucleus detail was visible on the long exposure navigation images they proved invaluable for dust coma studies. Figure 2 shows narrow jets, of angular size of a few degrees, in projection, viewed from two different solar phase angles.

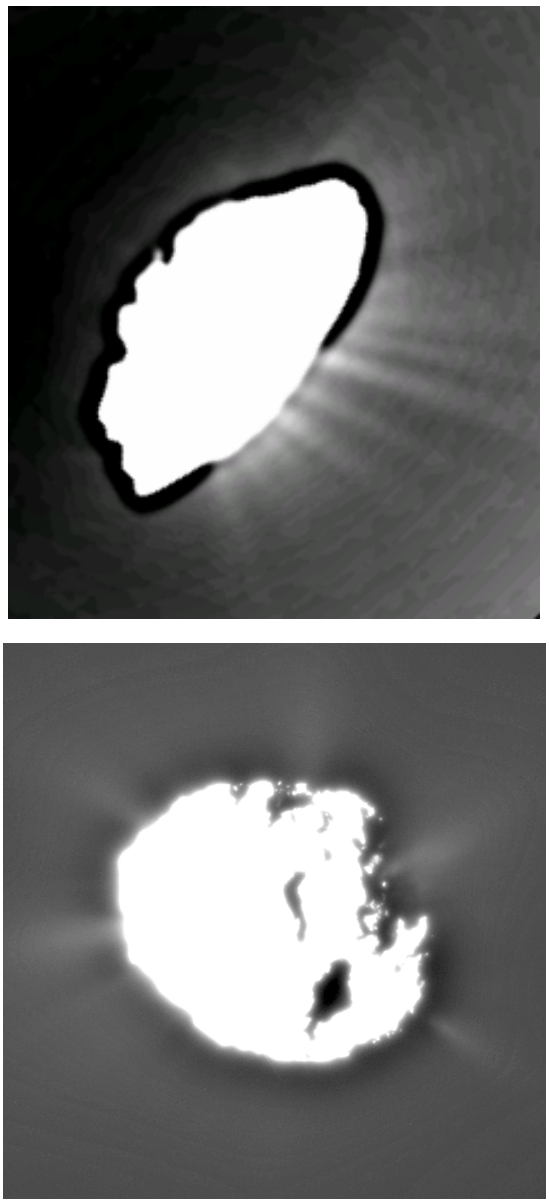

Figure 2. Long exposure navigation images of P/Wild 2 before and after closest approach showing narrow jets. In the upper image the Sun is to the lower right. In the lower image, with the Sun to the left, two jets to the right appear to emanate from unilluminated regions of the nucleus.

The science images have been used to define a shape model and rotation axis [11]. Three navigation images at different solar phase angles were then used to identify 20 jets and determine the distribution of their source locations on the surface [12]. Most of the jet sources were concentrated near the local equator with two (those seen in Fig. 2), active on the dark side of the nucleus. Assuming that dust production is continuous (at least while the source location is illuminated) the particles in the jets will trace out a thin conical sheet that may be traversed by Stardust during the flyby. Since the nucleus rotation period and the dust particle speeds are both unknown, only the *possibility* of jet traversal can be determined. Most of the concentrations of dust observed in the DFMI data (Sections 2.2 and 3.1) correspond to possible jet traversals.

2.2. DFMI fluxes

Although the DFMI became noisy during cruise operation, in-flight tests demonstrated nominal operation for at least 30 minutes after switch on. The instrument was therefore operated only for 30 minutes centred on the time of closest approach. The first dust detections were made by the front shield acoustic sensor, 264 s before closest approach (at a cometocentric distance r = 1630 km).

Almost 9000 impacts were detected, the majority, as expected, in the most sensitive channel of the small PVDF sensor. The acoustic sensors detected approximately 130 impacts with 7 penetrations of the front Whipple shield [13, 14], in line with pre-encounter expectations. What was not expected, however, was the spatial distribution of the dust. There was no smooth increase and decrease of the impact rate as the spacecraft passed through closest approach. Figure 3 illustrates the fluxes from the most sensitive channels of the PVDF and acoustic sensors throughout the encounter which are characterized by large variations over short timescales. Between 620 and 720 s after closest approach (3810 to 4420 km from the nucleus), very high fluxes were detected by the PVDF sensor, accounting for around 80% of all detected impacts. The last detected particle was at +922 s at a cometocentric distance of r = 5650 km.

2.3. DFMI mass distribution

Figure 4 shows the mass distribution derived for the period up to 600 s after closest approach. The cumulative mass distribution index α = 0.75 (where $N(>m) = k\, m^{-\alpha}$). The dust cross section is dominated by small particles, whereas the total mass is dominated by large particles. The estimated number of 15 μm particles captured in the aerogel (cross section 0.1 m^2) is 2300 ± 400 [13,14].

Figure 5 shows the mass distribution for the particles detected after 600s post encounter. Although they represent almost 80% of the total number of particles detected by DFMI, the much steeper mass distribution index of α = 1.13 means they contain only 3% of mass intercepting the spacecraft. The estimated number Estimated number of 15 μm particles in the aerogel collector from this region of the coma is 500 ± 200 [13,14].

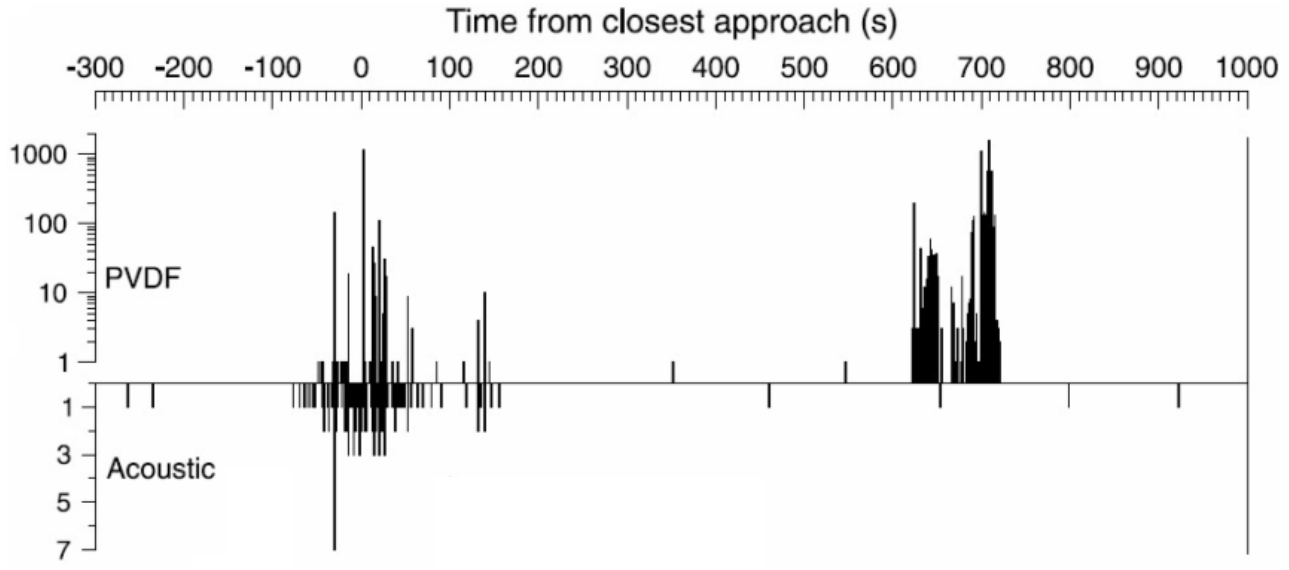

Figure 3. DFMI particle impacts per second throughout the 81P/Wild 2 encounter as measured in the most sensitive channels of the PVDF small area sensor (above axis) and the front shield acoustic A1 sensor (below axis).

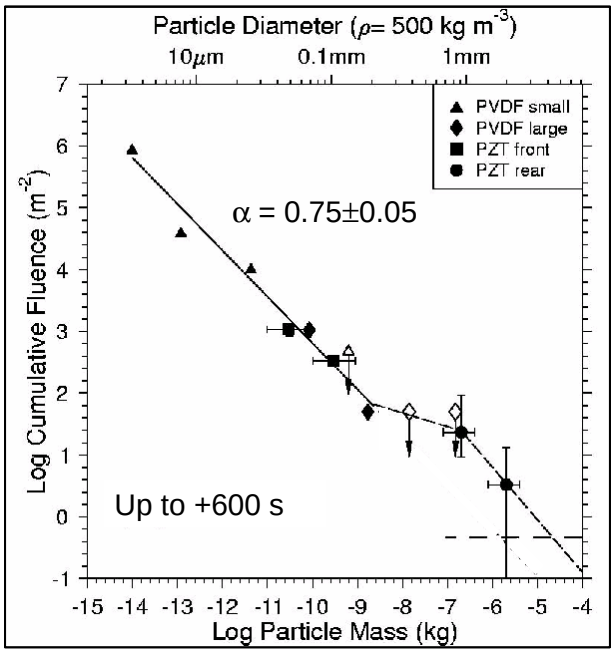

Figure 4. The fluence (time integrated flux) derived from DFMI data up to 600 s post-encounter. The horizontal dashed line corresponds to one impact on the spacecraft.

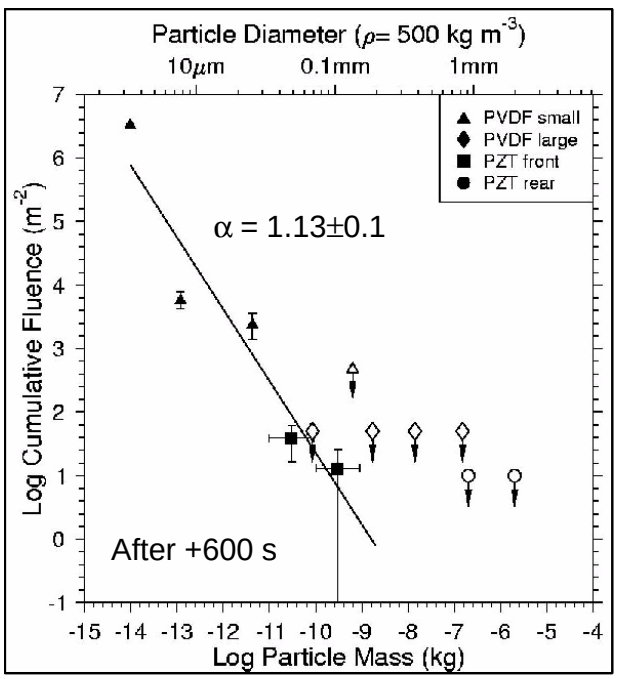

Figure 5. The fluence (time integrated flux) derived from DFMI data for the second period of particle detection after 600 s post-encounter.

The mass of largest particle impacting the spacecraft (not necessarily detected by DFMI) implied by the DFMI data is ~2×10^{-5} kg (diameter ~4 mm) [14] whereas the largest particle impacting the aerogel is predicted at ~6×10^{-7} kg (diameter ~1.3 mm) [13].

2.4. CIDA Fluxes

CIDA obtained 29 spectra during the comet flyby. The maximum event rate was always below 1 s^{-1} and the event counters also recorded 29 impacts [7]. This implies a fluence of $(3.3\pm0.6)\times10^{3}$ m^{-2}, a factor of about 1000 less than expected for consistency with the DFMI results (Figure 5), although the ratio of the rates between CIDA and the most sensitive DFMI channel DFMI, with a mass threshold about 10 times higher, is roughly constant. There is no evidence for any loss of sensitivity of CIDA, which would need to be a factor of ~10^{4} in mass to be consistent with DFMI. A more likely explanation appears to be a reduction in the effective area of the sensor, possibly due to shielding by some projection from the region of the front Whipple shields which are close to the line of sight of the CIDA target (Figure 1). The terminal speeds of micron sized particles detected by CIDA are likely to be a few hundred metres per second, resulting in a deviation from the spacecraft velocity vector of several degrees. Although the front shield was within 3º of the spacecraft velocity vector as seen by the CIDA target, it was located on the comet side of the spacecraft during encounter. The reason for the low apparent flux determined by CIDA is currently unknown.

2.5. Dynamic science results

At encounter there were no off-axis impacts of particles large enough to trigger firing of the 4.45 N thrusters, placing an upper limit of the largest impact on the Whipple shields covering the solar panels of $<10^{-4}$ kg One event was identified, at 15.5 s before closest approach, that triggered firing of the 0.89 N thrusters. The change in attitude means the particle must have impacted the main shield and had a mass in the range (2 to 4)$\times10^{-5}$ kg [15] consistent with the predicted largest impactor on the spacecraft from DFMI data.

3. JETS AND FRAGMENTATION

3.1. "Swarms" and "bursts"

Figure 6, shows fluxes measured in the most sensitive channel of the PVDF sensor at its highest time resolution of 0.1s for a period of 18 s immediately after closest approach. The fluxes show clustering on two timescales:

- 'Swarms' – timescales of seconds (~km)
- 'Bursts' – timescales of <1 s,
  and often <0.1 s (<600m)

The spatial dimensions of swarms are comparable with the angular sizes of jets observed in the near nucleus images. However, the changes in spatial density are far higher than would be expected within jets. No events were detected between –14 s and +1 s implying a mean

spatial density of less than 5×10^{-3} m^{-3}, whereas the peak between +1 and +2 s indicates a spatial density of > 400 m^{-3}.

Swarms are seen in both PVDF and acoustic sensor data and may be 'correlated' or 'anti-correlated' as shown in Figure 7. Particles emitted in jets would be expected to produce anti-correlated swarms. Differential gas drag acceleration of dust in the inner coma results in sorting of grains emitted at the same time from a jet source on the nucleus. This is effectively mass sorting although differences in shape have some effect. The 'garden sprinkler' effect produced by a rotating nucleus means that a spacecraft only samples particles in a jet that were emitted when the active region was at the sub-spacecraft point assuming radial outflow (as shown in Figure 8) or above the local surface normal for an irregular body.

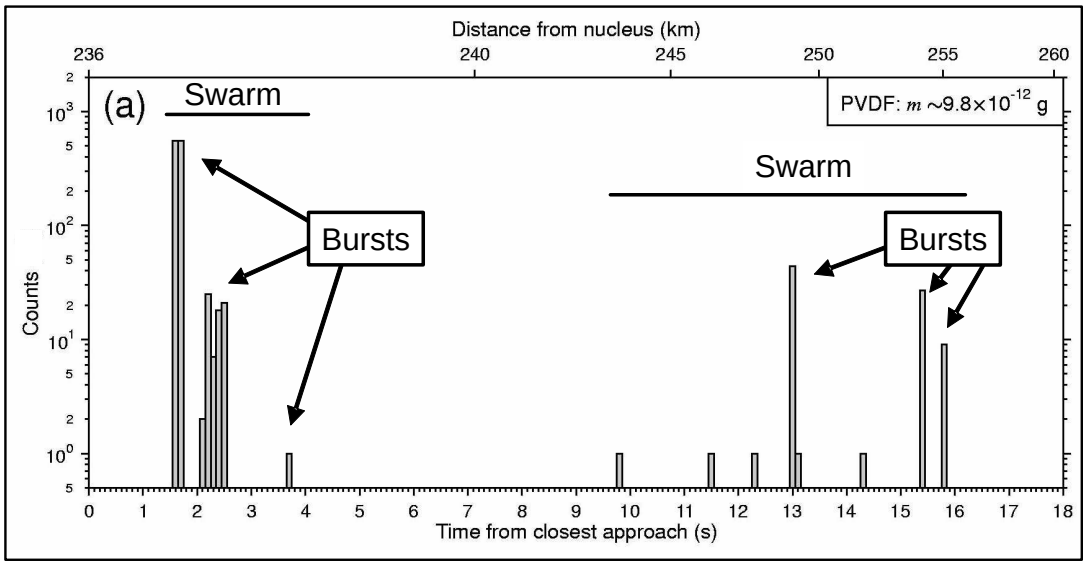

Figure 6. Impact counts in 0.1s intervals from the DFMI PVDF small sensor immediately after closest approach.

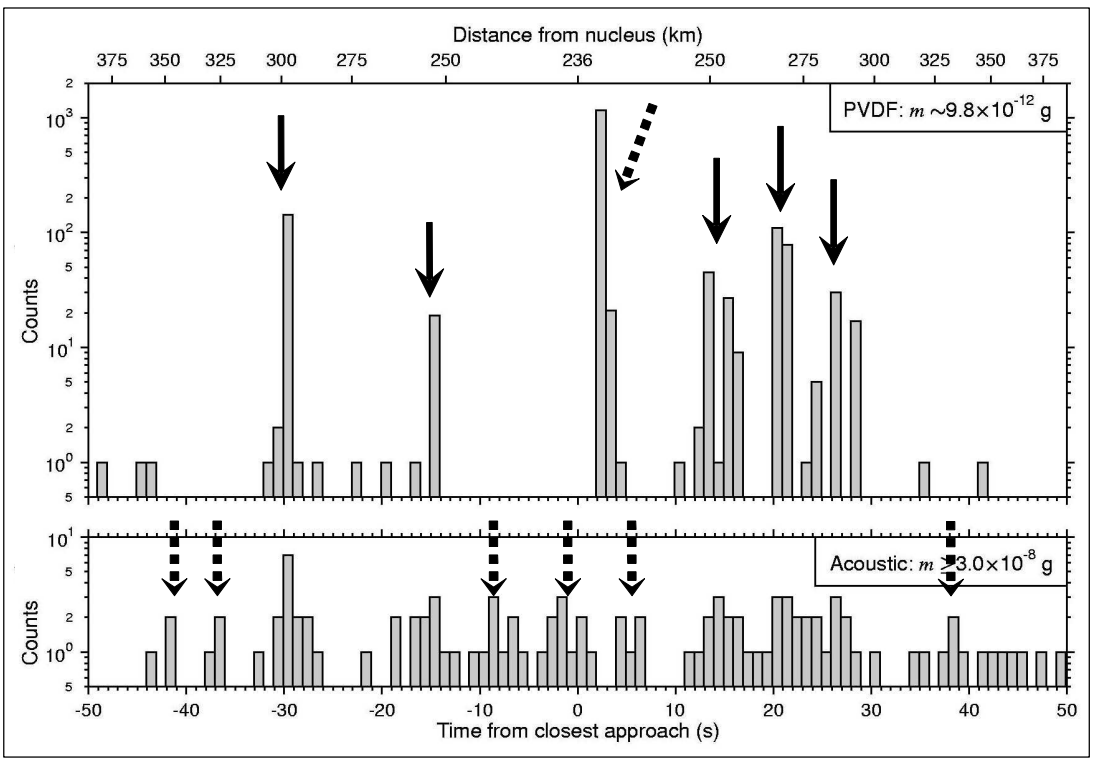

Figure 7. Impact counts in 1 second intervals measured by the DFMI PVDF small sensor (upper panel) and acoustic sensor A1 (lower panel) over a period of 100 s around closest approach. The solid and broken arrows show correlated and anti-correlated swarms respectively.

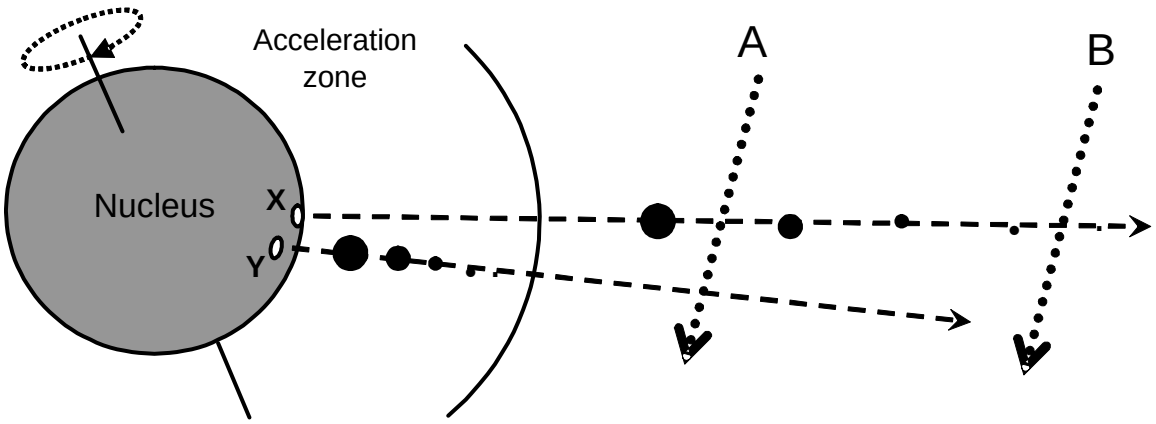

Figure 8. Schematic of mass sorting from an active region on a spherical rotating nucleus. A spacecraft on trajectory A will see a concentration of large grains emitted from a source when it was at position X, whereas a spacecraft on trajectory B will see small grains. Particles emitted earlier or later will not be seen unless the trajectory is in the same plane as the motion of the source.

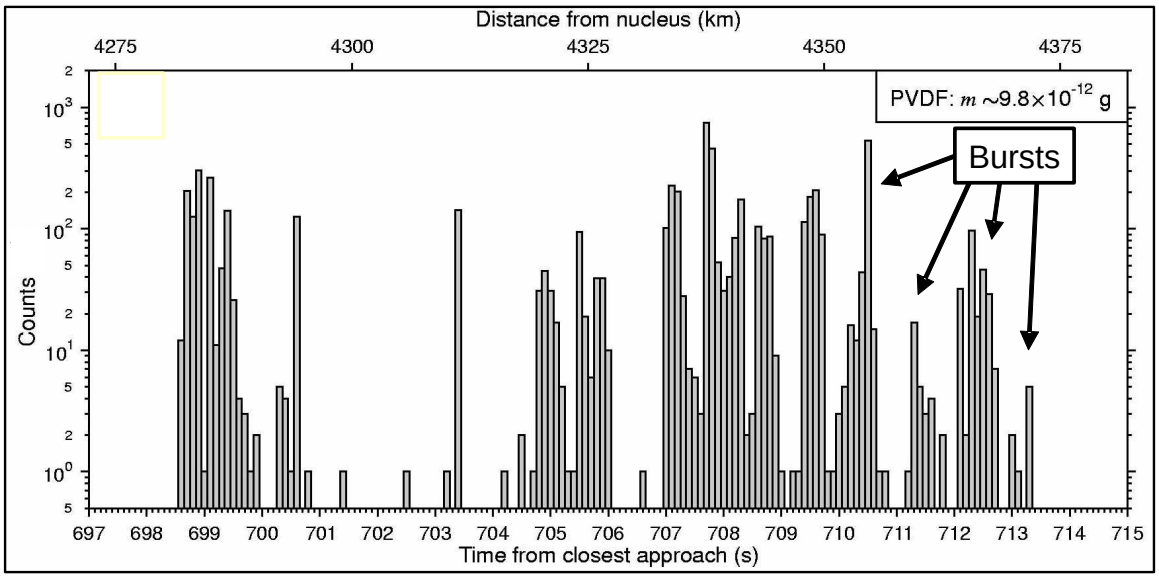

Figure 9. Impact counts in 0.1 second intervals measured by the DFMI PVDF small sensor during part of the late period of high impact rates.

Many swarms, however, have correlated large (acoustic) and small (PVDF) signals. In addition, the swarms are composed of 'bursts' with projected angular sizes at the nucleus of ~ 0.1° near nucleus, which do not match observed feature sizes in the images. The spatial density changes of factors greater than 1000 occur within the time resolution of 0.1 s (600 m). The late event also exhibits similar bursts (Figure 9) over 4000 km from the nucleus, which occur on timescales of 1 to 2 seconds, which correspond to even smaller angular sizes (~0.01°) when projected back to the nucleus.

3.2. Fragmentation

The only feasible explanation for the characteristics of these swarms and bursts is that fragmentation of grains occurs widely in the inner coma [13,14,16]. The bursts are particle clouds resulting from grain fragmentation:

- Anti-correlated swarms result from fragmentation close to the nucleus
- Correlated swarms result from fragmentation outside the acceleration zone

The local size distribution varies due to the stochastic fragmentation process but the overall mass distribution is an average of many jet crossings. Fragmentation clouds (bursts) are more likely to be crossed in jets (swarms).

The fragmentation process must be low energy to ensure that the clouds do not dissipate too quickly into the

coma. The later period of activity is interpreted as due to outgassing and/or fragmentation of a large boulder (diameter > 0.4 m) emitted before the most recent perihelion passage of the comet [12]. The location of this high period of activity is in the sector where large nucleus fragmentation products, leaving with very low relative speed, would be found [12]. The outgassing from such a fragment could provide a local source and the substructure would be a result of subsequent fragmentation of the emitted grains. Potential mechanisms and fragmentation modes are discussed in detail in [16].

3.3. Is Fragmentation the correct explanation?

The DFMI data and its interpretation have been met with some skepticism and a number of questions:

Q DFMI was noisy in interplanetary cruise; did it operate correctly at encounter?
A In cruise tests the noise occurred after >35 mins and noise produced continual PVDF counter overflows (cumulative count > 65535). The instrument operated nominally for 30 mins at the Annefrank flyby. All engineering data were nominal at the Wild 2 encounter and no PVDF counter overflows occurred (see [5] and [14] for further details).

Q Are the gaps in DFMI data real?
A No dead time or saturation effects were seen (PVDF dead time was ~μs allowing count rates of $>10^4$ s^{-1} with <5% dead time correction). The observed fluences were consistent with pre-encounter models and the total dust cross-section derived from ground-based observations). Fluences from independent subsystems are self-consistent (even though gaps in data are not coincident). If gaps in PVDF data are "filled in" the implied coma brightness would exceed observations by a factor of 100!

Q Jets do not result from active areas but are due to shocks resulting from non-radial gas flow due to coma shape. Therefore are not all dust features a natural result of gas dynamics and fragmentation is un-necessary?
A Stardust was always outside the inner coma but still detected coherent structures we can call jets, whatever their origin. Particle motions must be radial or near-radial to maintain these structures. Published gas dynamics models do not show spatial density enhancements larger than a factor of 2 and can only produce significant density enhancements for sub-micron dust since larger particles are not sufficiently well entrained in the gas flow.

Q Aren't the impacts at over 4000 km from the nucleus the result of the terminator shock predicted by gasdynamic models such as [17]?
A This structure is incompatible with a jet or terminator shock. Although it is in approximately the predicted location, it has a range of sub-structure that is inconsistent with either explanation and density changes far exceeding the predictions. Such high spatial densities require a much more powerful collimating mechanism or a local source. The location is consistent with a large boulder leaving from the nucleus with low relative velocity [12] and the substructure can result from subsequent fragmentation.

Q If fragmentation is occurring, how can there be detections of 50 μm particles but no 3 μm particles at certain times?
A Small and large particles are detected independently by two different subsystems of DFMI. Different effective areas for the different sensors (Table 1) result in different spatial density thresholds. Equal detection probabilities occur for the PVDF and acoustic sensors when the mass distribution index $\alpha = \sim 0.5$. The local mass distribution varies due to the mass sorting.

Q Why is this process not seen in other comets?
A Although previous dust experiments sampling the inner comae of comets did not have the sensitivity or time resolution to detect similar fragmentation process there is abundant indirect evidence (Section 3.4).

3.4. Evidence of fragmentation in other comets

The Giotto mission carried a dust instrument utilizing acoustic and impact plasma detectors which measured similar overall mass distributions at comet 1P/Halley [18] and 26P/Grigg-Skjellerup [19] as seen at 81P/Wild 2. The high encounter speed and low sampling rate at comet 1P/Halley meant that structures on the scale of those seen at Wild 2 would not have been detected [14].

The Vega 1 and Vega 2 flybys of comet Halley were much more distant, with closest approaches of >8000 km. However, the presence of mass separation in jets and 'clusters' and 'packets' were identified in the dust detector data (e.g. [20]).

The Optical Probe Experiment (OPE) observed the integrated scattered light from particles in its narrow field of view as it swept though the coma of comet 26P/Grigg-Skjellerup, and detected several short-lived increases in scattered light indicating enhanced dust spatial density in the field of view. Le Duin *et al.* [21] proposed an explanation in terms of expanding dust shells resulting from impacts directly onto the spacecraft structure. However, McBride *et al.* [22] showed that the data could not be matched by such a mechanism and proposed an alternative explanation as

detection of narrow jets and a possible large (10 – 100 m), outgassing or fragmenting, nucleus fragment over 1000 km from the nucleus.

Intensity profiles along narrow jets observed by Deep Space 1 in the inner coma of 19P/Borrelly showed intensity profiles that did not vary inversely with distance from the nucleus as would be expected for isotropic outflow. Although not a unique solution, the data were used to infer larger particles near the nucleus and the presence of fragmentation [23].

Fragmentation on large scales in cometary comae has been inferred from the presence of striae, seen in comet West (1975 VI-A) [24] and more recently, Hale-Bopp (1995-01).

Extended sources of gas emission seen in cometary comae may be a result of exposure due to fragmentation rather than the previously postulated process of slow sublimation [25].

The ejecta from the impactor of the Deep Impact mission at 9P/Tempel 1 consisted almost entirely of very small grains. The dominance of small particles implies that they were pre-existing either as very fine particles or as weak aggregates of such particles [26]. The extra energy in the impact would have caused instantaneous and complete fragmentation of aggregates that, in comet Wild 2 would have survived the more gentle gas drag lofting process.

4. CONCLUSION

The instruments on the Stardust spacecraft have revealed a highly heterogeneous dust coma during the flyby of 81P/Wild 2. Fragmentation is the only viable mechanism to explain the observed spatial density variations. The overall mass distribution was dominated by large particles but varied with position in the coma.

Similar structures appear to have been present in both 1P/Halley and 26P/Grigg-Skjellerup and there is abundant evidence for fragmentation in other comets. The overall coma properties in comets result from an average of highly variable local conditions. More extensive spatially and temporally resolved sampling together with measured particle velocities will be obtained by Rosetta at 67P/Churyumov-Gerasimenko.

The DFMI results predict the presence of 2800 ± 500 particles of diameter 15 μm or larger captured in the Stardust aerogel from a range of coma locations and sources. In addition to the detailed microanalysis of intact particles in the aerogel, impact craters in the aluminium foil covering the aerogel holder can be used to study the particle size distribution. The crater sizes are a function predominantly of grain size and speed (known) whereas the DFMI signals provide measurements of grain mass. Comparison between the two distributions could provide an independent determination of the original particle densities. This may be particularly useful if the particles have a loose aggregate structure similar to those seen in interplanetary dust particles captured in the stratosphere [27] which may fragment on impact into their sub-micron components.

5. REFERENCES

[1] Brownlee, D.E. et al. Stardust: comet and interstellar dust sample return mission, *J. Geophys. Res.*, 108, E10 8111, 15pp, 2003.

[2] Tsou, P., Brownlee, D.E., Sandford, S.A., Horz, F. and Zolensky, M. Wild 2 and interstellar sample collection and Earth return, *J. Geophys. Res.*, 108, E10 8113, 21pp, 2003.

[3] Grün, E., Gustafson, B., Mann, I., Baghul, G.E., Staubach, P., Taylor, A and Zook, H. Interstellar dust in the heliosphere, *Astron. Astrophys.*, 286, 915-924, 1994.

[4] Newburn, R.L., Bhaskaran, S., Duxbury, T.C., Fraschetti, G., Radey, T. and Schwochert, M., Stardust imaging camera, *J. Geophys. Res.*, 108, E10, 8116, 10pp, 2003.

[5] Tuzzolino, A. J. et al. Dust Flux Monitor Instrument for the Stardust mission to comet Wild 2, *J. Geophys. Res.*, 108, E10 8115, 24pp, 2003.

[6] Kissel, J. et al. Cometary and Interstellar Dust Analyzer for comet Wild 2, *J. Geophys. Res.*, 108, E10, 8114, 8pp, 2003.

[7] Kissel, J., Krueger, F.R., Silén, J. and Clark, B.C. The Cometary and Interstellar Dust Analyser at comet 81P/Wild 2, *Science*, 304, 1774-1776, 2004.

[8] Anderson, J.D., Lau, E.L., Bird, M.K., Clark, B.C., Giamperi, G. and Pätzold, M. Dynamic science on the Stardust mission, *J. Geophys. Res.*, 108, E10, 8117, 7pp, 2003.

[9] Tsou, P. et al. STARDUST encounters comet 81P/Wild 2, *J. Geophys .Res.* 109 E12S01, 8pp, 2004.

[10] Brownlee, D.E., Horz, F., Newburn, R.L., Zolensky, M., Duxbury, T.C., Sandford, S., Sekanina, Z., Tsou, P., Hanner, M.S., Clark, B.C., Green, S.F. and Kissel, J. Surface of Young Jupiter Family Comet 81P/Wild 2: View from the Stardust Spacecraft, *Science*, 304, 1764-1769, 2004.

[11] Duxbury, T.C., Newburn, R.L. and Brownlee, D.E. Comet 81P/Wild 2 size, shape, and orientation, *J. Geophys. Res*. 2004, 109, E12S02, 4pp, 2004.

[12] Sekanina, Z., Brownlee, D.E., Economou, T.E., Tuzzolino, A.J. and Green, S.F. Modeling the nucleus and jets of comet 81P/Wild 2 based on the Stardust encounter data, *Science*, 304, 1769-1774, 2004.

[13] Tuzzolino, A.J., Economou, T.E., Clark, B.C., Tsou, P. Brownlee D.E., Green, S.F., McDonnell, J.A.M., McBride, N. and Colwell, M.T.S.H. Dust measurements in the coma of comet 81P/Wild 2 by the Dust Flux Monitor Instrument, *Science*, 304, 1776-1780, 2004.

[14] Green, S.F., McDonnell, J.A.M., McBride, N., Colwell, M.T.S.H., Tuzzolino, A.J., Economou, T.E., Tsou, P., Clark, B.C. and Brownlee, D.E. Comet 81P/Wild 2 dust mass distribution, *J. Geophys. Res.*, 109 E12S04, 13pp, 2004.

[15] Anderson, J.D., Lau, E.L., Bird, M.K., Asmar, S.W., Clark, B.C., Giamperi, G., Gilliland, K. and Pätzold, M. Stardust dynamic science at comet 81P/Wild 2, *J. Geophys. Res.*, 109, E12S05, 7pp, 2004.

[16] Clark, B.C., Green, S.F., Economou, T.E., Sandfrod, S.A., Zolensky, M.E. and Brownlee, D.E. Release and fragmentation of aggregates to produce lumpy coma streams, *J. Geophys. Res.*, 109 E12S03, 13pp, 2004.

[17] Crifo. J-.F. and Rodionov, A.V. The dependence of the circum-nuclear coma structure on the properties of the nucleus, *Icarus*, 148, 464-478, 2000.

[18] McDonnell, J.A.M. et al. The dust distribution within the inner coma of comet P/Halley 1982i: Encounter by Giotto's impact detectors, *Astron. Astrophys.*, 187, 719-741, 1987.

[19] McDonnell, J.A.M., et al. Dust particle impacts during the Giotto encounter with comet Grigg-Skjellerup, *Nature*, 362, 732-734, 1993.

[20] Simpson, J.A., Rabinowitz, D., Tuzzolino, A.J., Ksanfomality, L.V. and Sagdeev, R.Z. The dust coma of comet 1P/Halley: measurements on the Vega-1 and Vega-2 spacecraft, *Astron. Astrophys.*, 187, 742-752, 1987.

[21] Le Duin, T., Crifo, J.F., Le Queau, D. & Crifo, F. A quantitative interpretation of the in-situ observations of the dust coma of comet P/Grigg-Skjellerup by the OPE photopolarimeter, *Astron. Astrophys.*, 308, 261-272, 1996.

[22] McBride, N., Green, S.F., Levasseur-Regourd, A.-C., Goidet-Devel, B. and Renard, J.-B. The inner dust coma of comet 26P/Grigg-Skjellerup: multiple jets and nucleus fragments? *Mon. Not. R. Astron. Soc.*, 289, 535-553, 1997.

[23] Boice, D.C., Britt, D.T., Nelson, R.M., Sandel, B.R., Soderblom, L.A., Thomas, N. and Yelle, R.V. The near-nucleus environment of 19P/Borrelly during the DS-1 encounter, *Proc. Lunar Planet Sci. Conf.*, 33, Abs. 1810, 2002.

[24] Sekanina, Z. and Farrell, J.A. Evidence for fragmentation of strongly nonspherical dust particles in the tail of comet West 1976 VI, in *Solid Particles in the Solar System*, ed. I. Halliday, Springer, New York, 267-270, 1980.

[25] Gunnarson, M, Rickman, H,, Festou, M.C., Winnberg, A. and Tancredi, G. An extended CO source around comet 29P/Schwassman-Wachmann 1, *Icarus*, 157, 309-322, 2002.

[26] A'Hearn, M.F. et al. Deep Impact: Excavating Comet Tempel 1, *Science*, 310, 258 – 264, 2005.

[27] Brownlee, D.E. Cosmic dust: collection and research. *Ann. Rev. Earth Planet. Sci.*, 13, 147-173, 1985.

ACKNOWLEDGEMENTS

The Open University acknowledge the financial support of the UK Particle Physics and Astronomy Research Council.